

# Birefringence of AlGaAs/GaAs Coatings under Above-Band-Gap Illumination, GR Noise and Photo-Optic Transfer Function

Bin Wu,<sup>1,\*</sup> Shreyan Goswami,<sup>1</sup> Satoshi Tanioka,<sup>2</sup> and Stefan Ballmer<sup>1</sup>

<sup>1</sup>*Department of Physics, Syracuse University, Syracuse, New York 13244, USA*

<sup>2</sup>*School of Physics and Astronomy, Cardiff University, Cardiff CF24 3AA, United Kingdom*

(Dated: December 2, 2025)

AlGaAs/GaAs coatings are being considered as coating candidates for gravitational-wave detectors. In this paper we investigate the birefringence properties of this crystalline semiconductor material by modulating the optical illumination on the mirror coating and monitoring the induced birefringence. While the measured low-frequency birefringence values align with previous studies, we observed a frequency-dependent behavior in the illumination-to-birefringence coupling, characterized by a pole increasing with illumination intensity and a DC gain decreasing with illumination intensity. We developed a theoretical mode based on a master equation to characterize the measurement results by considering photon-induced electric fields and electro-optical effects. This model reproduces the frequency and intensity dependencies of the induced birefringence. Additionally, this model predicts a generation-recombination noise (GR noise) will be observable in the coatings birefringence. While the presented measurement cannot predict the exact level of GR noise, for the frequency band and spot sizes relevant for gravitational-wave detectors we expect GR noise to be white below the pole frequency, scale with power the same way laser shot noise does, and for fixed power be independent of spot size.

PACS numbers:

## I. INTRODUCTION

Currently, the sensitivity of ground-based gravitational-wave detectors is limited by thermal noise from optical test mass coatings at around 100 Hz [1–3]. The fluctuation-dissipation theorem directly connects this thermal noise to the mechanical dissipation [4, 5] and thermal dissipation [3, 6, 7] in the optical coatings. Today, these coatings are dielectric stacks of sputtered amorphous materials, alternating between the Ti-doped Ta<sub>2</sub>O<sub>5</sub> and SiO<sub>2</sub> [8].

A very promising alternative are AlGaAs/GaAs crystalline coatings, which exhibit extremely low intrinsic mechanical dissipation [9–11]. Indeed, the lowest thermal noise reference cavities to-date use this coating [12]. In these crystalline semiconductor coatings electric field fluctuations cause a birefringence, i.e. a difference in the reflected field phase between s- and p- polarization, which mimics as mirror motion for a single polarization [13, 14]. Moreover, the semiconductor band structure implies that under high optical intensities charge carriers can be excited. Even for photon energies below the material bandgap this can still happen via multi-photon processes. Also band-bending at the coating interface structure can lead to trapping of charge carriers near the coating [15]. This can result in changes in the internal electric field across the coating, and therefore changes in the phase of light reflected off the coating. Since the effect has opposite sign for p- and s- polarization, this coupling can be measured by comparing the resonant frequency of the

two polarizations in a cavity.

According to JILA's results, the static birefringence in AlGaAs coating is  $n_{\text{biref}} \approx 7 \times 10^{-4}$  [16], where  $n_{\text{biref}}$  refers to the static refractive index difference between the two polarizations. They also observed that  $n_{\text{biref}}$  depends on the intracavity light intensity. Similar results are obtained when the coatings are illuminated with above-band-gap photons [17].

In this paper we study the dynamic birefringence change introduced by light-induced charge carriers in the semiconductor coating. We built an optical cavity with one Al<sub>0.92</sub>Ga<sub>0.08</sub>As/GaAs mirror and measured the transfer functions from the above-band-gap illumination to the birefringent line splitting between two orthogonal polarizations under different DC powers. In addition, to study the wavelength dependence of external illumination, we used two different light sources: 700 nm (higher than the bandgap of GaAs but lower than that of AlGaAs) and 430 nm (higher than the bandgaps of both GaAs and AlGaAs), and varied the intra-cavity carrier (1064 nm) intensity. Based on the measured result, we provide a simple master equation model describing how the illumination and the intra-cavity laser intensity affect the birefringence level. This model predicts the photo-optic transfer function, that is the intensity-to-phase coupling for the AlGaAs/GaAs coating. Finally, the master equation theory predicts the existence of generation-recombination (GR) noise. We derive the power spectrum density of the birefringence GR noise, which also gives us the noise scaling with optical power and spot size.

---

\*Electronic address: bwu127@syr.edu

## II. EXPERIMENT DESIGN

Birefringence results in a frequency splitting ( $f_{\text{biref}}$ ) between the linearly polarized fast and slow eigenmodes of an optical cavity. The frequency splitting is proportional to the birefringence angle of the coating,  $\phi_{\text{biref}}$ , and to the cavity free spectral range,  $\text{FSR} = \frac{c}{2L}$ , where  $c$  denotes the speed of light and  $L$  is the cavity length:

$$f_{\text{biref}} = \text{FSR} \times \frac{\phi_{\text{biref}}}{2\pi}. \quad (1)$$

Thus the shorter the cavity, the larger the frequency splitting. But a short cavity also results in a small beam spot and therefore a comparatively high 1064 nm beam intensity. We wanted to keep the intensity below about  $5\text{ MW/m}^2$  to reduce the impact of below-band-gap light and chose the input laser power and cavity parameters listed in Table I accordingly. The output coupler of our cavity is an  $\text{Al}_{0.92}\text{Ga}_{0.08}\text{As}/\text{GaAs}$  mirror with 81 aperiodic layers and is optimized to minimize thermo-optic noise for 1064 nm [18]. While varying the aluminum-to-gallium ratio can yield different electrical and optical properties, the coating we used has been demonstrated to exhibit low mechanical loss and high optical quality, meeting the standard requirements for gravitational-wave detectors [11]. We measured a static frequency splitting of about 1 MHz, corresponding to a birefringence angle  $\phi_{\text{biref}} = 1.7 \times 10^{-3}$ , within the range of literature values [2].

TABLE I: Cavity and coating parameters.

Parameter	Value
Cavity length	4 cm
Free spectral range	3.75 GHz
Finesse (measured)	$\sim 500$
FWHM linewidth	7.8 MHz
Beam spot $w$ on coating	0.3 mm
1064 nm intracavity power range	$2.0 - 3.7 \text{ MW/m}^2$
Input coupler reflectivity	98.8% at 1064 nm
Output coupler reflectivity ( $\text{Al}_{0.92}\text{Ga}_{0.08}\text{As}/\text{GaAs}$ coated)	99.99% at 1064 nm

The setup of the experiment is shown in FIG. 1. Two lasers with different polarizations are locked to a 4-cm short cavity simultaneously using PDH locking [19] with sidebands at 25 MHz and 45 MHz respectively. A half-wave plate is placed right before the cavity to rotate the p- and s- modes to align them with the fast and slow axes of the crystalline coating. Additionally, the beat note between the two lasers is measured by a photodiode, and either directly recorded at 10 MHz sampling rate, or, to simplify transfer function measurements, fed into a phase-locked loop. The control signal of that phase-locked loop is a direct measurement of the introduced frequency shift.

Two LEDs (700 nm and 430 nm) are driven from 1 Hz to 10 kHz with a fixed DC offset. Any birefringence

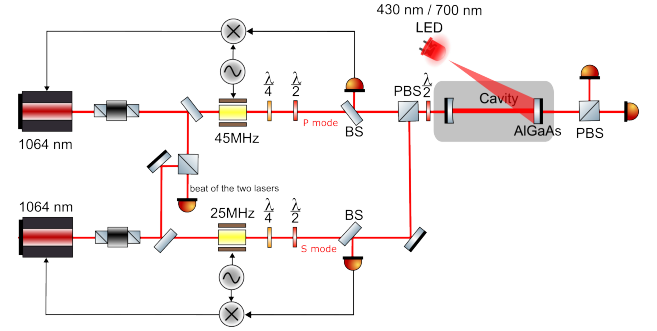


FIG. 1: Experiment Scheme. The optical cavity is 4-cm long, with its output coupler coated with  $\text{Al}_{0.92}\text{Ga}_{0.08}\text{As}/\text{GaAs}$ . To monitor the frequency splitting between orthogonal polarizations induced by the illumination, we measured the beat note between two independent lasers, one locked to the cavity in p- polarization and the other in s- polarization.

induced by the illumination will modulate the beat note frequency of the two polarizations. The amplitude of the introduced beat note frequency shift  $\Delta f_{\text{induced}}$  is given by

$$\Delta f_{\text{induced}} = \text{FSR} \times \frac{\Delta\phi_{\text{biref}}}{2\pi}, \quad (2)$$

where  $\Delta\phi_{\text{biref}}$  denotes the illumination-induced birefringent angle.

## III. MEASUREMENT RESULTS

A phase-locked loop (PLL) was implemented to track the beat note between the two lasers. The coupling coefficients from illumination to coating birefringence were determined from the transfer function between the LED drive and the PLL control signal, followed by a series of calibrations. This section presents the main measurement results for different illumination conditions. Details of the measurement scheme and calibration are provided in Appendix C.

### A. Frequency dependence

FIG. 2 shows a typical transfer function, which indicates that the coupling coefficient from the illumination to the induced birefringence is frequency dependent. Here, the LED wavelength is 700 nm and the intensity is  $1.5 \text{ W/m}^2$  with a modulation of  $1 \text{ W/m}^2$ , corresponding to a modulation index of  $m = 0.67$ . The amount of modulation was chosen to get a relatively higher signal-to-noise ratio and does not change the coupling values. The transfer function exhibits two main features: a flat gain at DC and a single-pole roll-off at around 300 Hz. The pole frequency suggest a  $1/e$  lifetime of a few hundred microseconds for the relevant

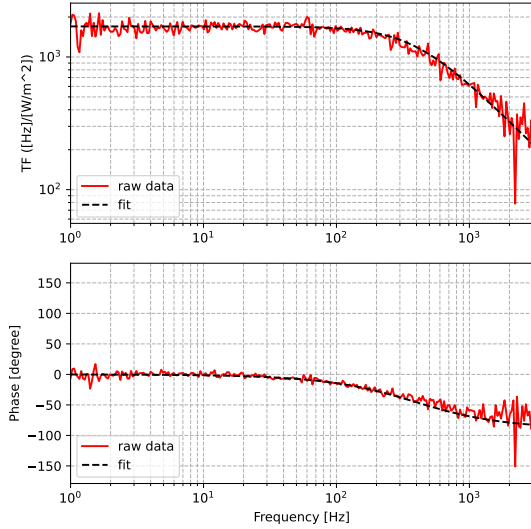


FIG. 2: Typical transfer function from LED illumination to beat note noise. The solid line shows the raw data and the dashed line is a fitting to a first-order low-pass filter. 1064 nm intensity:  $2.0 \text{ MW/m}^2$ , LED wavelength: 700 nm, LED intensity:  $1.5 \text{ W/m}^2$  DC, plus a modulation of  $\pm 1 \text{ W/m}^2$  (modulation index  $m = 0.67$ ).

excited carriers in the coating. Both the phase and amplitude of the measurement data can be well fitted to a first-order low-pass filter. We lose coherence above around 2 kHz, which is largely due to insufficient gain of the laser locking loops.

The DC value of the transfer function FIG. 2 is around  $1.7 \times 10^3 \text{ Hz/(W/m}^2)$ . We can convert this into an induced phase shift using the FSR of our cavity:

$$\Delta\phi = 2\pi \frac{\Delta f}{\text{FSR}} = 2\pi \frac{1.7 \times 10^3 \text{ Hz/(W/m}^2)}{3.75 \text{ GHz}} I, \quad (3)$$

$$\frac{\Delta\phi}{I} = 2.8 \times 10^{-6} \text{ rad/(W/m}^2). \quad (4)$$

We can compare this with JILA's results, especially the data shown in the right plot of Fig.4 in [17]. Since we modulate the illumination while they fix the intensity for each measurement, our measurement corresponds to the slope of theirs. It is clear that the slope of the line splitting in their results decreases as the light intensity increases. Furthermore, the coupling coefficients derived from their results are in the range of  $10^{-6} \sim 10^{-5} \text{ rad/(W/m}^2)$ . Note that their cavity carrier wavelength is 1550 nm, and the LED illumination wavelengths are different from ours.

### B. Change in illumination intensity

To study the effect of intensity level on the coupling coefficient, we then changed the DC power of the

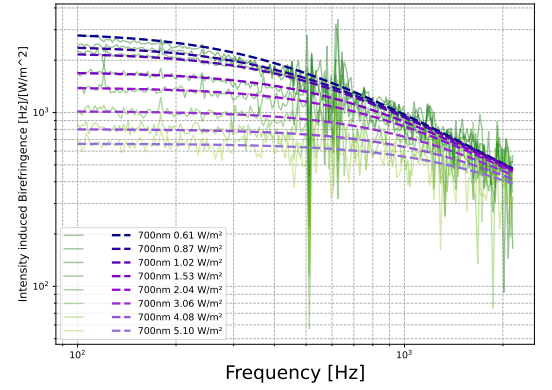


FIG. 3: Fitting results at different illumination intensity levels: The wavelength of the illumination is 700 nm. The solid green lines are measured raw data after calibration. The noise peaks at  $\sim 500 \text{ Hz}$  and  $\sim 600 \text{ Hz}$  are due to the mechanical resonance of the cavity mirror posts. The dashed lines are the fitting results obtained by the four-parameter global fit described in section IV A and appendix A. This plot shows data for a 1064 nm carrier light intensity of  $2.0 \text{ MW/m}^2$ . See FIG. 6 (a) and (b) for other 1064 nm intensities.

illumination. The results of multiple measurements are shown in FIG. 3. The solid lines are measured raw data and the dashed lines are the fitting results obtained by the four-parameter global fit described in section IV A and appendix A below. We find that as the intensity increases, the coupling coefficient decreases and the pole frequency increases. More specifically, in FIG. 3 as the DC intensity  $I_1$  of the 700 nm LED varies from  $0.6 \text{ W/m}^2$  to  $5.1 \text{ W/m}^2$ , the DC coupling levels decrease from 2760 to 660  $\text{Hz/(W/m}^2)$ , consistent with the functional fit  $\propto (I_{\text{ref}} + I_1)^{-1}$ . Above the rising pole frequency, the dependence of the transfer function on the external illumination intensity level is much reduced and consistent within the measurement noise to be independent of the illumination intensity. Thus the pole frequency can be fitted by the linear function  $\propto (I_{\text{ref}} + I_1)$  with the same  $I_{\text{ref}}$ .

The red dots in FIG. 4 show the DC values in FIG. 3. The yellow and green dots correspond to different levels of 1064 nm intra-cavity intensity - see FIG. 6 and section III C.

### C. Change in cavity carrier intensity

The wavelength of the carrier in our experiment is 1064 nm, which is below the bandgap of AlGaAs and GaAs. However, below-band-gap illumination can also excite charge carriers and thus induce birefringence through two-photon absorption on a time scale much shorter than our observations. Indeed FIG. 4 shows that higher carrier intensities result in lower DC gain values. The dashed lines are predicted values from the global fit

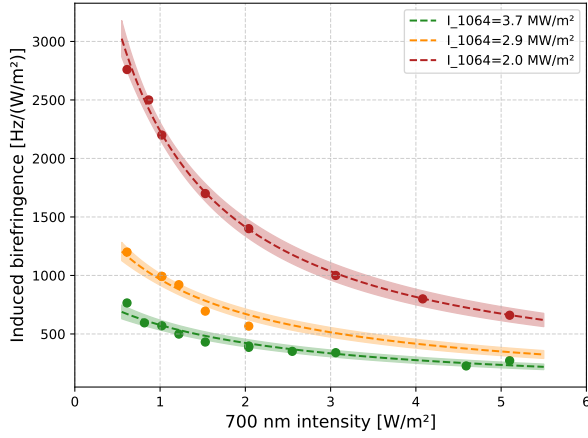


FIG. 4: DC gain values for the induced birefringence under various of 700 nm and 1064 nm intensities. The x-axis is the intensity of 700 nm illumination and different colors represent varying 1064 nm intensities. The data points come from the measurements shown in FIG. 3 and FIG. 6. The dashed lines and shaded uncertainties are calculated based on the model described in Appendix A.

model described in section IV A and appendix A, and the shaded area shows the uncertainty range.

#### D. Comparison between 700 nm and 430 nm illumination

700 nm illumination is above the band gap of GaAs but below the band gap of AlGaAs. To see the difference when AlGaAs is also activated, we swapped the LED from 700 nm to 430 nm, and then ran the same measurement.

FIG. 5 shows the results when the coating is illuminated with a 430 nm LED. Overall, the response was similar to the results obtained from 700 nm illumination: flat at lower frequencies and roll-offs at higher frequencies. However, the differences are also obvious. First, at similar intensity levels, the DC gain of the induced birefringence under 430 nm illumination is several times lower than that under 700 nm illumination. This could be explained by the large fraction of 430 nm incident power being absorbed by the top GaAs layer of the coating [20]. Secondly, the fitted model for the 430 nm measurement is a superposition of a series of pole frequencies rather than a single low-pass filter. This suggests that the distribution of effective lifetimes of the involved carriers is spread out, an effect we would expect if for example the carrier lifetime depends significantly on the 1064 nm intensity, which in turn varies across the readout beam spot. Additionally, since the photon energy of the 430-nm laser can excite carriers in both GaAs and AlGaAs, the lifetime differences and interactions between the layers may also account for the

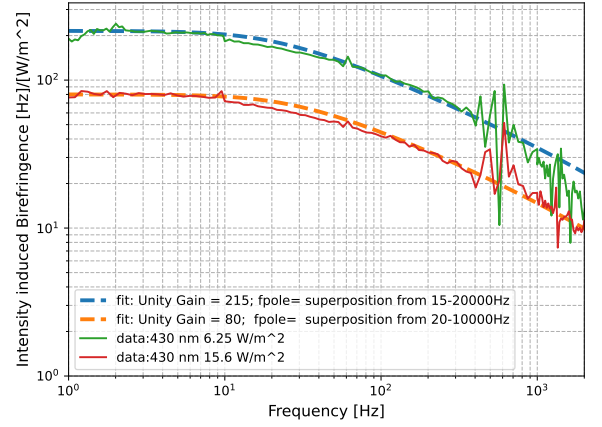


FIG. 5: Transfer functions from 430 nm LED intensity to beat note noise. Solid lines represent measurement data under different illumination intensities. Dashed lines indicate fitted curves for the raw data. Each of the fitted curves here is not simply a pure first-order low-pass filter, but consists of a series of superimposed first-order low-pass filters. This is the expected response if the distribution of effective lifetimes of the involved carriers is spread out.

observed pole superposition.

Because our 700 nm data was much cleaner, both in terms of single pole frequency and overall signal-to-noise, we did not include the 430 nm data in the global fit presented in Table II and the noise models presented below.

## IV. MASTER EQUATION AND NOISE

### A. Global Fit to Master Equation

The behavior of the measurement results presented in sections III A through III C can be captured by a master equation model for the number of charge carriers  $N$  across the effective area responsible for an induced charge area density  $\sigma = e N/A$  trapped near the coating layers, which in turn causes birefringence through the electro-optical effect [13]. Here  $e$  is the elementary charge, and  $A$  is the effective area. Details are described in appendix A. The master equation up to linear order in  $(N - \bar{N})$  can be written as (see equation 29):

$$\dot{N} = -\Gamma(I_i) (N - \bar{N}(I_i)), \quad (5)$$

where  $I_i$  is the photon flux intensity of the illuminations at 1064 nm ( $i = 0$ ) and 700 nm ( $i = 1$ ), and  $\bar{N}(I_i)$  is the equilibrium number of charge carriers. This model predicts a simple pole transfer function

$$\delta\phi_{\text{biref}} = \frac{2\eta C_{EO}^{\text{ext}} e}{\epsilon_0 A} \frac{g_{\text{DC}}}{1 + i\omega/\Gamma} \delta I_1, \quad (6)$$

where

$$g_{DC} = \frac{\bar{N}}{\partial \bar{I}_1}(\bar{I}_i) \quad \text{and} \quad \Gamma = \Gamma(\bar{I}_i). \quad (7)$$

Here  $C_{EO}^{\text{ext}}$  is the measured coating response to external electric fields [14], the factor 2 accounts for both polarizations (fast minus slow),  $\eta < 1$  is a coupling efficiency describing how much weaker the coating response is to electric fields from the photo-generated charge carrier distribution, and  $\epsilon_0$  is the vacuum permittivity. We can in principle measure the full functions  $g_{DC}(\bar{I}_i)$  and  $\Gamma(\bar{I}_i)$ . For our dataset we were able to get a relatively good fit for these two functions with just four parameters  $\Gamma_0$ ,  $a_0$ ,  $a_1$  and  $K_{10}$ :

$$\Gamma = \Gamma_0 + a_0 \bar{I}_0 + a_1 \bar{I}_1, \quad (8)$$

$$g_{DC} = \frac{K_{10}}{\Gamma(\bar{I}_0, 0)\Gamma(\bar{I}_i)} = \frac{K_{10}}{\Gamma_0 + a_0 \bar{I}_0} \cdot \frac{1}{\Gamma_0 + a_0 \bar{I}_0 + a_1 \bar{I}_1}, \quad (9)$$

where we can interpret the parameters as the spontaneous decay rate  $\Gamma_0$  (although the best fit results in a negative number), the two cross sections for photo-induced recombination (or excitation to a non-participating energy level)  $a_i$ , and an overall gain  $K_{10}$ . Similarly,  $g_{DC}\Gamma/A = K_{10}/\Gamma(\bar{I}_0, 0)/A$  is the capture probability for  $i=1$  photons, and  $I_{\text{ref}} = (\Gamma_0 + a_0 \bar{I}_0)/a_1$  is the reference intensity mentioned before.

**Global Fitting Results**

Name	Parameter	Value
Spontaneous decay rate	$\Gamma_0$	$-908 \text{ s}^{-1}$
Recomb. cross sections 1064 nm	$a_0$	$1.96 \times 10^{-22} \text{ m}^2$
Recomb. cross sections 700 nm	$a_1$	$4.79 \times 10^{-16} \text{ m}^2$
Gain	$\eta K_{10}/A$	$0.80 \text{ s}^{-1}$
Capture probability 700 nm	$\eta g_{DC}\Gamma/A$	
$(\bar{I}_0 = 2.0 \text{ MW/m}^2)$		$6.58 \times 10^{-4}$
$(\bar{I}_0 = 2.9 \text{ MW/m}^2)$		$3.74 \times 10^{-4}$
$(\bar{I}_0 = 3.7 \text{ MW/m}^2)$		$2.71 \times 10^{-4}$

TABLE II: Result from global fit to master equation.  $\eta$  is the coupling efficiency of the excited charge carrier, compared to external electric fields, see equation 34. The fit values for  $\eta K_{10}/A$  also assume  $C_{EO}^{\text{ext}} = 1.3 \times 10^{-10} \text{ rad/(V/m)}$ , the measured coating response to external electric fields [14].

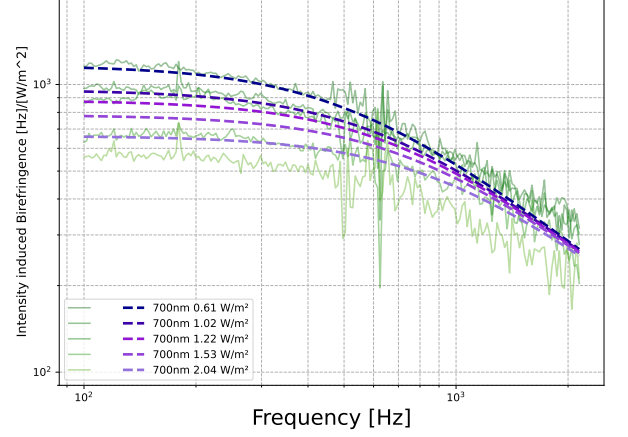
Our experiment is only sensitive to the product  $C_{EO}K_{10} = C_{EO}^{\text{ext}}\eta K_{10}$ . Thus we only report values for the combination  $\eta K_{10}$ . The results from a global fit for the model parameters are shown in Table II. The table also includes values for the capture probabilities  $\eta g_{DC}\Gamma/A$  at the 1064 nm intensities  $(\bar{I}_0)$  where we captured our data.

We already mentioned that we can expect the coupling efficiency  $\eta$  to be less than one. Our measurement also suggests a lower limit: Since  $g_{DC}\Gamma/A$  is the capture probability for photons, it has to be less than one, which in turn means that  $\eta$  is bounded below by the largest

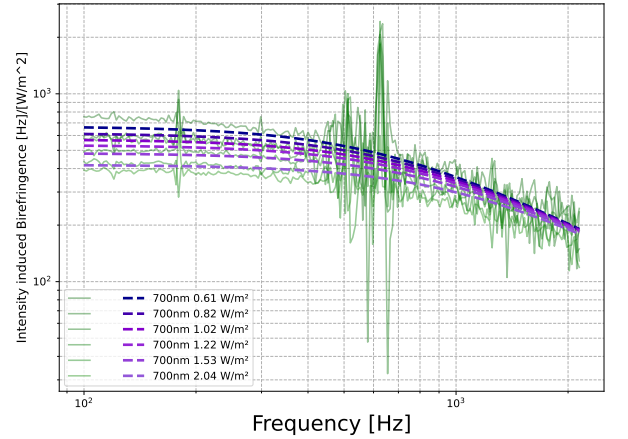
measured value for the measured value for  $\eta g_{DC}\Gamma/A$  in table II:

$$6.58 \times 10^{-4} \times \frac{1.3 \times 10^{-10} \text{ rad/(V/m)}}{C_{EO}^{\text{ext}}} < \eta < 1. \quad (10)$$

Here we included the explicit dependence of the result in table II on the previously measured  $C_{EO}^{\text{ext}}$ .



(a) 1064 nm intensity = 2.9 MW/m<sup>2</sup>.



(b) 1064 intensity = 3.7 MW/m<sup>2</sup>.

FIG. 6: Single global fit for two sets of data with different illumination situations. Dashed lines are direct low-pass fitting from the raw data. Solid lines are calculated from the global model introduced in Appendix A. This model reproduces the frequency-dependent low-pass shape of the transfer functions and also shows that the DC coupling values and pole frequencies shift with the illumination intensity.

## B. Photo-Optic Transfer Function and Noise

While we measured the transfer function from above-band-gap intensity modulation to birefringence observed at the 1064 nm carrier wavelength, the master equation model 15 is symmetric in the indices  $i =$

1,2. We thus can also predict the transfer function from 1064 nm carrier light to birefringence, that is the intensity-to-phase coupling due to the coating. That transfer function has the same pole frequency  $\Gamma/(2\pi)$ , see equation 36. The strength of that coupling is dependent on an integration constant, which we did not measure in our experiment. However, that strength could be predicted using the pole frequency measured here and tracking the DC behavior of the birefringence as a function of the 1064 nm light intensity, as done for instance in [16].

### C. Generation-Recombination Noise

The master equation 15 or 29 is a probabilistic process. Thus, there is a shot noise associated with the generation and recombination of charge carriers. This is known in the literature as GR noise [21]. The expected GR noise one-sided displacement power spectral density  $S_{\delta x^2, \text{GR}}^{\text{one-s}}$ , as well as the photo-optic noise driven by intensity noise  $S_{\delta x^2, \text{PO}}^{1-s}$  is derived in appendix B (equation 46):

$$S_{\delta x^2, \text{GR}}^{1-s} = \left( \frac{\lambda}{4\pi} \frac{C_{EO}^{\text{ext}} e}{A \epsilon_0} \right)^2 \frac{4\eta^2(\Gamma\bar{N} + r)}{\Gamma^2 + \omega^2}, \quad (11)$$

$$S_{\delta x^2, \text{PO}}^{1-s} = \left( \frac{\lambda}{4\pi} \frac{C_{EO}^{\text{ext}} e}{A \epsilon_0} \right)^2 \frac{(\eta K_i \bar{I}_i)^2 S_{\text{RIN}_i}^{1-s}}{\Gamma^2 + \omega^2}. \quad (12)$$

$S_{\text{RIN}_i}^{1-s}$  is the relative intensity noise one-sided power spectral density, which drives the photo-optic noise. While equation 11 cannot predict the magnitude of the GR noise because we do not know the integration constant in  $\bar{N}$  and the value of  $r(\bar{N})$ , it does predict the spectral shape and scaling of GR noise (see appendix A equation 48): In words, below the pole frequency  $\Gamma/(2\pi)$  the GR noise is *white*, scales with power *the same way laser shot noise does*, and is *independent of the spot size A* for constant power  $\bar{P}_0$ , as long as the spot radius is larger than the Debye length  $\lambda_D$ . Remarkably, no other known displacement noise in the observation band of gravitational-wave interferometers is white, making this a signature hallmark of GR noise.

## V. DISCUSSIONS

The observed transfer function can be intuitively explained by considering the density and lifetime of states trapped near the coating interface layers in AlGaAs/GaAs coatings. Photons absorbed by the coating can excite charge carriers to these states. In addition, the lifetime of these states is affected by incident light, with higher intensities shortening the lifetime. The time evolution of the charge carrier density then determines the shape of the transfer function: On time scales shorter than the lifetime, the occupation level is the integral of the illumination intensity, resulting in

a  $1/f$  transfer function roughly independent of intensity. On time scales longer than the lifetime, any increase in occupation level due to higher illumination intensities is suppressed by the shortened lifetime of the states.

The pole frequency is thus determined by the effective carrier lifetime:  $f_p = \Gamma/(2\pi)$ . Based on our measurements, the effective lifetime of the induced charge carriers is on the order of a few hundred microseconds. This is longer than what could be expected from the natural decay of a semiconductor. There are several possible mechanisms that can account for the long lifetime of photo-induced charge carriers. The fact that the band gaps of GaAs and AlGaAs are different leads to band bending [15]. The conduction band of GaAs bends downward, forming a 2D potential well that traps electrons and makes it harder for recombination. In addition, DX centers (deep donors) in the AlGaAs barriers act as metastable traps, further prolonging the carrier lifetime and resulting in persistent photoconductivity [22, 23]. This effect is temperature dependent, since thermal energy can assist electrons to return into the DX centers, thereby quenching the persistence.

Table III lists the mean laser power intensity on the test masses of different gravitational-wave detectors, together with the estimated pole frequency of the intensity-to-phase transfer function and the GR noise. Note that in all cases the pole frequency is above the observation band, that is, the shortened lifetime due to the high intensity helps to suppress the intensity noise coupling. However, the same suppression is not available for GR noise, as both the generation and recombination rates still increase.

TABLE III: Mean laser intensity and GR pole frequency for different gravitational-wave detectors.

Detector	Laser intensity [kW/cm <sup>2</sup> ]	Pole frequency [kHz]
aLIGO	4.5	7.4
LIGO A+	9.1	15
LIGO A#	17	28
CE	3.3	5.4

Our model further reveals two light-induced noise sources for crystalline coatings (equation 11 and 12): the photo-optic noise which is driven by the laser intensity noise, and the GR noise which is a kind of shot noise scaling inversely with the laser power below the pole frequency. We are unable to predict the magnitude of those two noise sources because in this experiment we only modulated the LED illumination intensity. Also, the coupling coefficient ( $\eta$ ) remains hard to determine. Finally note that the coupling coefficient of the external electric fields in [14] is obtained in the 20-40 kHz frequency band, whereas our range of interest lies below 10 kHz.

All the results obtained in this paper are from the same



coating sample. We would like to test different samples with identical coatings to make it more convincing that the observed characteristics represent universal properties of AlGaAs/GaAs coatings.

## VI. CONCLUSION

In this paper, light-induced birefringence is investigated for  $\text{Al}_{0.92}\text{Ga}_{0.08}\text{As}/\text{GaAs}$  coating under different illumination conditions. By measuring the transfer functions from the illumination to the beating frequency between the s- and p- polarizations, we observed a frequency dependence of the illumination to birefringence coupling coefficient: flat at lower frequencies and roll-off at higher frequencies. The DC values and pole frequencies are determined by both the outside LED illumination intensity and the carrier intensity. There is a clear trend showing that higher illumination intensities result in lower DC gains and higher pole frequencies for the transfer functions. The measured DC response is consistent with previous research, while the high-frequency roll-off characteristic is observed for the first time.

Considering the processes of carrier generation and decay as well as the electro-optic effect, we proposed a theoretical model to describe the measurement results. Overall, our model reproduces the low-pass trend and intensity dependence of the transfer functions.

Further research is required to refine the model. In the current experiment, we were unable to modulate the carrier intensity (1064 nm) and measured only three sets of data with different carrier intensities. As a result we cannot with certainty extrapolate the carrier intensity data much beyond our data range ( $I_0$  between 2.0 and 3.7  $\text{MW}/\text{m}^2$ ). Additionally, investigating the temperature dependence of induced birefringence would be valuable, as it may provide clues as to whether photon-phonon interactions are involved.

## VII. ACKNOWLEDGMENT

The work in this paper was supported by the National Science Foundation award PHY-2513058 and PHY-2309296. We would also like to thank Professors Martin Fejer, Garrett Cole and Steven Penn for many fruitful discussions. This paper was assigned the LIGO DCC number LIGO-P2500676.

# Appendices

## A. A THEORETICAL MODEL FOR LIGHT INDUCED BIREFRINGENCE

To model the observed birefringence dependence on illumination sources, we assume that the birefringence change  $\Delta\phi_{\text{biref}}$  is caused by the local electric field change  $\Delta E$  of a charge carrier population trapped in or near the coating:

$$\Delta\phi_{\text{biref}} = 2C_{EO}\Delta E = \frac{2C_{EO}}{\epsilon_0}\Delta\sigma, \quad (13)$$

with  $\epsilon_0$  the vacuum permittivity and  $\Delta\sigma$  the change in the carrier area density causing the electric fields across the coating. The electro-optical coupling coefficient  $C_{EO}$  encodes the response of the coating to the particular field configuration caused by trapped charge carrier density, and the factor 2 accounts for both polarizations (fast minus slow).

We are interested in the time evolution and noise of this carrier area density  $\sigma(t)$ . Thus we express  $\sigma(t)$  in terms of the number of participating charge carriers  $N(t)$ , elementary charge  $e$  and an effective area  $A$ :

$$\sigma(t) = \frac{e}{A}N(t). \quad (14)$$

If the 1064 nm readout radius  $w$  is much larger than the Debye length  $\lambda_D$  for transverse diffusion,  $A$  is simply the 1064 nm readout beam spot area  $\pi w^2$ . If  $w \ll \lambda_D$ ,  $A$  is the carrier transverse diffusion area  $\approx \pi\lambda_D^2$ . If  $w$  and  $\lambda_D$  are comparable,  $A$  is a diffusion-enlarged spot size. Since we chose a very large illumination spot, effectively uniform illumination,  $A$  does not matter for the transfer function calculation, but it will matter for noise considerations.

The time evolution of the number of charge carriers  $N(t)$  is in general governed by a master equation (see for instance [21]):

$$\dot{N} = -R(N, I_i) + G(N, I_i) = F(N, I_i). \quad (15)$$

$G(N, I_i)$  is the charge carrier generation rate, and  $R(N, I_i)$  is the recombination rate (including excitation to a non-participating state). Both  $G$  and  $R$  in general depend on the population  $N$  itself, as well as the illuminating external optical photon flux intensity  $I_i$ . In the model we explicitly include the 1064 nm carrier intensity  $I_0$ , and the 700 nm carrier intensity  $I_1$ .

To simplify notation, we also introduce the function  $F(N, I_i) = G(N, I_i) - R(N, I_i)$  for the right side of the master equation. For constant external fields  $I_i$  the system will settle at a mean carrier number  $\bar{N}(I_i)$ , defined by

$$F(\bar{N}(I_i), I_i) = 0. \quad (16)$$

Using the chain rule this constraint implies

$$\frac{\partial \bar{N}}{\partial I_1}(I_i) = -\frac{\frac{\partial F}{\partial I_1}(\bar{N}(I_i), I_i)}{\frac{\partial F}{\partial \bar{N}}(\bar{N}(I_i), I_i)}. \quad (17)$$

In our experiment, the 1064 nm carrier intensity is fixed, i.e.,  $I_0$  is time independent, while the 700 nm illumination  $I_1(t)$  is modulated. We can thus perform a perturbative expansion of the master equation 15:

$$N(t) = \bar{N} + \delta N(t), \quad \text{with} \quad |\delta N(t)| \ll \bar{N}, \quad (18)$$

$$I_0 = \bar{I}_0, \quad (19)$$

$$I_1(t) = \bar{I}_1 + \delta I_1(t), \quad \text{with} \quad |\delta I_1(t)| \ll \bar{I}_1. \quad (20)$$

We thus obtain the linearized equation:

$$\delta \dot{N}(t) = \frac{\partial F}{\partial \bar{N}}(\bar{N}, \bar{I}_i) \delta N(t) + \frac{\partial F}{\partial I_1}(\bar{N}, \bar{I}_i) \delta I_1(t) \quad (21)$$

$$= -\Gamma(\bar{N}, \bar{I}_i) \delta N(t) + K_1(\bar{N}, \bar{I}_i) \delta I_1(t), \quad (22)$$

with the effective decay rate

$$\Gamma(\bar{N}, \bar{I}_i) = -\frac{\partial F}{\partial \bar{N}}(\bar{N}, \bar{I}_i), \quad (23)$$

and the effective generation rate

$$K_i(\bar{N}, \bar{I}_i) = \frac{\partial F}{\partial I_i}(\bar{N}, \bar{I}_i). \quad (24)$$

The frequency domain response function is thus given by

$$\frac{\delta N}{\delta I_1} = \frac{K_1}{\Gamma + i\omega} \quad (25)$$

$$= \frac{g_{\text{DC}}}{1 + i\omega/\Gamma}. \quad (26)$$

This corresponds to a simple pole transfer function with pole frequency

$$f_p = \frac{\Gamma}{2\pi}, \quad (27)$$

and DC gain

$$g_{\text{DC}} = \frac{K_1}{\Gamma} = \frac{\partial \bar{N}}{\partial I_1}, \quad (28)$$

as we should expect since  $\bar{N}$  is the equilibrium carrier number.

Finally, to interpret our experimental data, it is desirable to Taylor-expand the master equation 15 up to linear order in  $N$  around  $\bar{N}(I_i)$ :

$$\dot{N} = -\Gamma(I_i)(N - \bar{N}(I_i)) + (g - r), \quad (29)$$

with  $(g - r) = O((N - \bar{N})^2)$ . The remainder terms are defined via

$$R = \Gamma(I_i)N + r(N, I_i), \quad (30)$$

$$G = \Gamma(I_i)\bar{N}(I_i) + g(N, I_i). \quad (31)$$

Equation 29 is indeed consistent with equations 16 to 28. Moreover our experiment directly measures  $\Gamma(I_i)$  and the derivative  $\frac{\partial}{\partial I_1}\bar{N}(I_i) = g_{\text{DC}}(I_i)$ , up to an uncertain coupling coefficient  $C_{EO}$ .

Finally we note that the leading term  $\Gamma N$  looks like a good guess for the entire recombination rate  $R$ . But strictly speaking we cannot assume  $r(\bar{N}) = 0$ , which becomes relevant for noise calculations. However we do know that  $r(\bar{N}) = g(\bar{N})$ .

To fit our dataset we fit the two measurable functions  $\Gamma(\bar{I}_i)$  and  $g_{\text{DC}}(\bar{I}_i)$  with four parameters: the spontaneous decay rate  $\Gamma_0$ , the two cross sections for photo-induced recombination (or excitation to a non-participating energy level)  $a_i$ , and an overall gain  $K_{10}$ :

$$\Gamma = \Gamma_0 + a_0\bar{I}_0 + a_1\bar{I}_1, \quad (32)$$

$$g_{\text{DC}} = \frac{K_{10}}{\Gamma(\bar{I}_0, 0)\Gamma(\bar{I}_i)} = \frac{K_{10}}{\Gamma_0 + a_0\bar{I}_0} \cdot \frac{1}{\Gamma_0 + a_0\bar{I}_0 + a_1\bar{I}_1}. \quad (33)$$

Note that  $K_1 = g_{\text{DC}}\Gamma = K_{10}/\Gamma(\bar{I}_0, 0)$  is the capture cross section for  $i=1$  photons, see equation 22.

Finally, in equation 13, we do not know the true electro-optical coupling coefficient  $C_{EO}$  for the particular field configuration caused by trapped charge carrier density we are dealing with. We only know the coefficient for external fields,  $C_{EO}^{\text{ext}} = 1.3 \times 10^{-10} \text{ rad}/(\text{V}/\text{m})$ , measured in [14]. We expect the relevant coupling  $C_{EO}$  to be somewhat smaller than  $C_{EO}^{\text{ext}}$ , so we can write

$$C_{EO} = \eta C_{EO}^{\text{ext}}, \quad (34)$$

with  $\eta < 1$ , a coupling efficiency due to the geometry of the electric fields from the charge carrier distribution. Our transfer function experiment cannot distinguish changes in  $\eta$  from changes in  $K_{10}$ , so we only report values for  $\eta K_{10}$  for the fitting results presented in Table II. However, knowledge of  $\eta$  will become important for GR noise estimation presented below.

We can also integrate our fit (equation 33) and get an explicit form for the  $\bar{N}(I_i)$  and therefore for the master equation in terms of our fitted parameters

$$\dot{N} = -\Gamma \left( N + \frac{K_{10}}{a_1\Gamma_1} (\ln \Gamma - \ln \Gamma_1) - \bar{N}_0 \right), \quad (35)$$

where we introduced the abbreviation  $\Gamma_1 = \Gamma(I_0, 0)$ , and as expected we cannot determine the integration constant  $\bar{N}_0(I_0)$ .

Finally, we note that the master equation 15 is symmetric in the fields  $I_0$  and  $I_1$ , thus, by swapping the indices 0 and 1, we also find the shape of the intensity-to-phase coupling of the coating for the 1064 nm light:

$$\frac{\delta N}{\delta I_0} = \frac{K_0}{\Gamma + i\omega}. \quad (36)$$

This 1064 nm transfer function will have the same pole frequency as the measured 700 nm light. While we did



not measure the magnitude of this coupling  $K_0$ , it could be predicted by just tracking the DC behavior of the birefringence.

## B. GR-NOISE AND PHOTO-OPTIC NOISE

To understand the noise implications of our model we return to the most general form of the master equation 15, written in terms of generation terms  $G$  and recombination terms  $R$ :

$$\dot{N} = -R(N, I_i) + G(N, I_i). \quad (37)$$

The fluctuations in  $N$  are fundamentally due to two processes:

1. The generation  $G$  and recombination  $R$  each are probabilistic processes that can only generate or destroy a whole charge carrier. Thus, each contributes a shot noise ( $\delta R$  and  $\delta G$  respectively) with (1-sided) amplitude spectral density equal to  $\sqrt{2G(\bar{N}, I_i)}$ . The literature refers to this noise as Generation-Recombination noise, abbreviated as GR noise. To calculate the GR noise for our situation, we can follow the description of GR noise in semiconductors outlined in [21].
2. Intensity fluctuations in the drive fields  $I_i$  will couple to the birefringence with the transfer function derived in appendix A (equation 26 and 36). We will refer to this coupling as photo-optic noise.

First, we note that we can write the (1-sided) amplitude spectral density for the source terms  $\delta R$  and  $\delta G$  as

$$\sqrt{2G(\bar{N}, I_i)} = \sqrt{2R(\bar{N}, I_i)} = \sqrt{2\Gamma\bar{N} + 2r(\bar{N}, I_i)}, \quad (38)$$

where  $r(\bar{N}, I_i)$  is the remainder term introduced in equation 30. Next, to calculate GR noise, we can again perform a perturbative expansion

$$N = \bar{N} + \delta N, \quad (39)$$

$$I_0 = \bar{I}_0 + \delta I_0, \quad (40)$$

$$I_1 = \bar{I}_1 + \delta I_1, \quad (41)$$

and explicitly add the driving noise terms  $\delta R$  and  $\delta G$ :

$$\delta \dot{N} = -R + G - \delta R + \delta G \quad (42)$$

$$= -\Gamma\delta N + K_i\delta I_i - \delta R + \delta G, \quad (43)$$

We thus find

$$\delta N = \frac{K_i\delta I_i - \delta R + \delta G}{\Gamma + i\omega}. \quad (44)$$

We can now write the 1-sided power spectral density for fluctuations  $\delta N$  as

$$S_{\delta N^2}^{1-s} = \frac{(K_i\bar{I}_i)^2 S_{\text{RIN}_i^2}^{1-s} + 4(\Gamma\bar{N} + r)}{\Gamma^2 + \omega^2}. \quad (45)$$

where  $S_{\text{RIN}_i^2}^{1-s}$  is the 1-sided power spectral density of the relative intensity noise for the  $I_i$  field, and the rate power spectral density of  $\delta R$  and  $\delta G$  are given by the square of equation 38.

We can now cast this into an effective 1-sided displacement noise power spectral density for the coating

$$S_{\delta x^2}^{1-s} = \left( \frac{\lambda}{4\pi} \frac{C_{EO}^{\text{ext}}}{A \epsilon_0} e \right)^2 \frac{(\eta K_i \bar{I}_i)^2 S_{\text{RIN}_i^2}^{1-s} + 4\eta^2(\Gamma\bar{N} + r)}{\Gamma^2 + \omega^2}, \quad (46)$$

where we also reintroduced  $\eta$  and the measured coupling for external electrical fields  $C_{EO}^{\text{ext}}$  via  $C_{EO} = \eta C_{EO}^{\text{ext}}$ .

**Noise Scaling:** We expect the GR noise to be spatially correlated up to the Debye length  $\lambda_D$  due to transverse diffusion, but uncorrelated across the coating for larger separations. Note that for fixed intensities  $I_i$  both  $K_i$  and  $\bar{N}$  are proportional to the effective area  $A$ . This guarantees that for fixed intensities  $I_i$  photo-optic noise is independent of  $A$ , while for the GR noise we have

$$S_{\delta x^2, \text{GR}}^{1-s} \propto \frac{1}{A} \text{ for fixed intensities } I_i. \quad (47)$$

Finally, we need to look at the scaling of GR noise with power in the frequency band of interest for gravitational-wave detectors, roughly 10 Hz to 1 kHz. For typical operating powers of gravitational-wave detectors our frequency band lies below the pole frequency and we have  $\Gamma \approx \Gamma_1 \approx a_0 \bar{I}_0$ . In this approximation the GR noise is entirely driven by the unmeasured integration constant  $\bar{N}_0$  and remainder term  $r$ . To nevertheless predict a power scaling, we have to *assume* that the generation rate  $G = \Gamma\bar{N} + r$  is proportional to the total power  $\bar{P}_0 = A\bar{I}_0$  on the optic. Here  $A$  is the beam spot area, which for gravitational-wave detectors is much bigger than the diffusion area. Thus we find

$$S_{\delta x^2, \text{GR}}^{1-s} \propto \frac{1}{A\bar{I}_0} = \frac{1}{\bar{P}_0}, \quad (48)$$

where  $\bar{P}_0$  is the total power on the coating (the interferometer arm power). In words, below the pole frequency the GR noise is *white*, scales with power *the same way laser shot noise does*, and is *independent of the beam spot area  $A$*  for constant power  $\bar{P}_0$ .

## C. CALIBRATION

In order to measure the LED illumination to birefringence transfer functions we locked both the s- and p- modes of the cavity using Pound-Drever-Hall

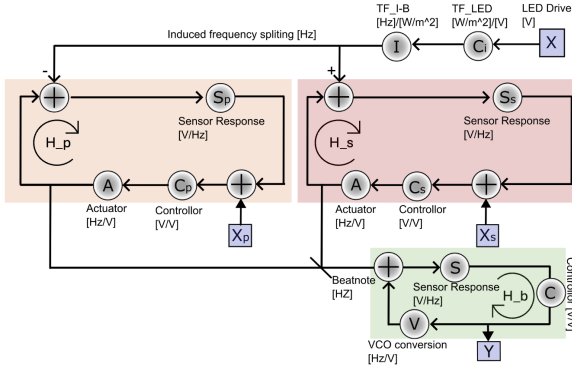


FIG. 7: Block diagram of the experimental setup. Color-coded are the s- and p- polarization control loops (orange and red), as well as the PLL loop (green) tracking the beat note.

(PDH) control loops. The beat signal of the two laser polarizations was fed into a phase-locked loop (PLL) to lock the output of a voltage-controlled oscillator (VCO) to the beat note signal, as shown in FIG. 7. The control signal sent to the VCO is a direct measure of the beat note frequency.

### 1. PDH Locking Loops for the Two Polarizations

The laser locking sensing responses  $S_s$  and  $S_p$  can be obtained from the error signal in the PDH locking process. The slope of the error signal linear range corresponds to the sensing gain. It varied between 6 V/GHz and 18 V/GHz, depending on the laser input power. The measurement was repeated for every data run.

### 2. Transfer Functions

The LED drive ( $X$ ) is first converted to the LED light intensity and then induces a birefringent frequency shift for the two orthogonal modes, in a different direction.  $H_p$  and  $H_s$  in the diagram denote the locking loop gains of two orthogonal modes.  $H_b$  denotes the gain of the PLL. The transfer function from illumination to birefringence, which is written as  $I$  in the block diagram, can then be calculated from the following measurement results.

We first inject an excitation signal from the laser locking error signal node ( $X_p$  or  $X_s$ ), and then measure the transfer function from the error signal node to the VCO control signal  $Y$ . Let us take the P-mode locking loop as an example: the transfer function  $\frac{Y}{X_p}$  can be calculated by the following when the cavity noise is relatively small:

$$\frac{Y}{X_p} = \frac{1}{1 - H_p} \times C_p \times A \times \frac{1}{1 - H_b} \times S \times C, \quad (49)$$

$$= \frac{H_p}{1 - H_p} \times \frac{1}{S_p} \times \frac{1}{1 - H_b} \times S \times C, \quad (50)$$

in which  $C_p$  and  $S_p$  are the controller and sensor response of the p mode locking loop;  $A$  is the laser actuator response and  $C$  is the PLL controller.

The second step is to measure the transfer function from the LED drive  $X$  to VCO control signal  $Y$ :

$$\frac{Y}{X} = C_i I \times \left( \frac{H_p}{1 - H_p} + \frac{H_s}{1 - H_s} \right) \times \frac{1}{1 - H_b} \times S \times C, \quad (51)$$

where  $C_i$  indicates the LED conversion from drive voltage to the illumination intensity and  $S$  is the sensor response of PLL. Now with equation 50 and equation 51, we find that:

$$I = \frac{1}{C_i} \times \frac{Y}{X} \times \frac{1}{\left( S_s \frac{Y}{X_s} + S_p \frac{Y}{X_p} \right)}. \quad (52)$$

In the case where  $H_p \gg 1$ ,  $H_s \gg 1$ ,  $S_p \approx S_s$  we then find

$$I = \frac{1}{S_p} \times \frac{X_p}{Y} \times \frac{1}{2C_i} \times \frac{Y}{X}. \quad (53)$$

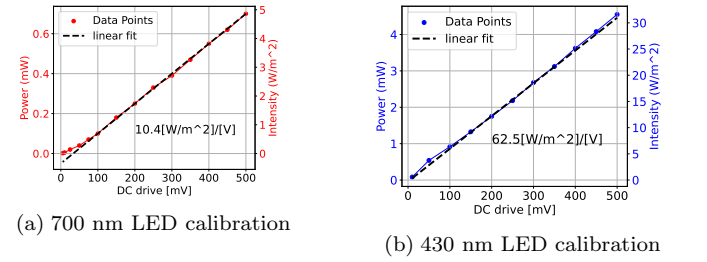


FIG. 8: LED calibration. For the 700 nm LED, we have: 10.4 [W/m<sup>2</sup>]/[V] and for the 430 nm LED, we have: 62.5 [W/m<sup>2</sup>]/[V].

### 3. LED Illumination Calibration

The LED conversion from drive voltage to illumination intensity is shown in Fig. 8. The external illumination sources at 700 nm and 430 nm were incident under approximately 45 degrees to the mirror surface. Throughout this paper we report the illumination intensity without correcting for the angle cosine or for the effective coating reflectivity at that angle and wavelength. We also measured the LED's frequency response using a photodetector that collects scattered light, see Fig. 9 for an example. The gain fluctuations were within  $\pm 1\%$ .

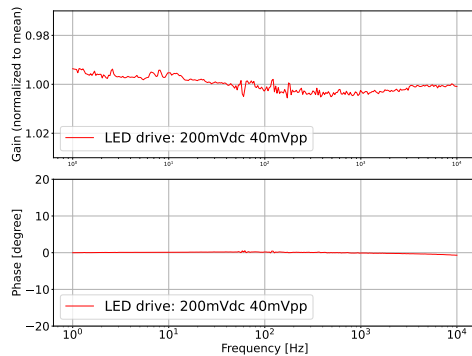


FIG. 9: Frequency response of the 700 nm LED measured with a drive source of 200 mV DC voltage and 40 mV peak-to-peak modulation from 1 to 10 kHz. The gain value is normalized to mean and the fluctuations are less than  $\pm 1\%$ . Crucially, the transfer function is flat up to 10 kHz without any roll-off pole.

- 
- [1] E. Capote, W. Jia, N. Aritomi, M. Nakano, V. Xu, R. Abbott, I. Abouelfettouh, R. X. Adhikari, A. Ananyeva, S. Appert, S. K. Apple, K. Arai, S. M. Aston, M. Ball, S. W. Ballmer, D. Barker, L. Barsotti, B. K. Berger, J. Betzwieser, D. Bhattacharjee, G. Billingsley, S. Biscans, C. D. Blair, N. Bode, E. Bonilla, V. Bossilkov, A. Branch, A. F. Brooks, D. D. Brown, J. Bryant, C. Cahillane, H. Cao, F. Clara, J. Collins, C. M. Compton, R. Cottingham, D. C. Coyne, R. Crouch, J. Csizmazia, A. Cumming, L. P. Dartez, D. Davis, N. Demos, E. Dohmen, J. C. Driggers, S. E. Dwyer, A. Effler, A. Ejlli, T. Etzel, M. Evans, J. Feicht, R. Frey, W. Frischhertz, P. Fritschel, V. V. Frolov, M. Fuentes-Garcia, P. Fulda, M. Fyffe, D. Ganapathy, B. Gateley, T. Gayer, J. A. Giaime, K. D. Giardina, J. Glanzer, E. Goetz, R. Goetz, A. W. Goodwin-Jones, S. Gras, C. Gray, D. Griffith, H. Grote, T. Guidry, J. Gurs, E. D. Hall, J. Hanks, J. Hanson, M. C. Heintze, A. F. Helmling-Cornell, N. A. Holland, D. Hoyland, H. Y. Huang, Y. Inoue, A. L. James, A. Jamies, A. Jennings, D. H. Jones, H. B. Kabagoz, S. Karat, S. Karki, M. Kasprzack, K. Kawabe, N. Kijbunchoo, P. J. King, J. S. Kissel, K. Komori, A. Kontos, Rahul Kumar, K. Kuns, M. Landry, B. Lantz, M. Laxen, K. Lee, M. Lesovsky, F. Llamas Villarreal, M. Lormand, H. A. Loughlin, R. Macas, M. MacInnis, C. N. Makarem, B. Mannix, G. L. Mansell, R. M. Martin, K. Mason, F. Matichard, N. Mavalvala, N. Maxwell, G. McCarrol, R. McCarthy, D. E. McClelland, S. McCormick, T. McRae, F. Mera, E. L. Merilh, F. Meylahn, R. Mittleman, D. Moraru, G. Moreno, A. Mullavey, T. J. N. Nelson, A. Neunzert, J. Notte, J. Oberling, T. O'Hanlon, C. Osthelder, D. J. Ottaway, H. Overmier, W. Parker, O. Patane, A. Pele, H. Pham, M. Pirello, J. Pullin, V. Quetschke, K. E. Ramirez, K. Ransom, J. Reyes, J. W. Richardson, M. Robinson, J. G. Rollins, C. L. Romel, J. H. Romie, M. P. Ross, K. Ryan, T. Sadecki, A. Sanchez, E. J. Sanchez, L. E. Sanchez, R. L. Savage, D. Schaetzl, M. G. Schiowski, R. Schnabel, R. M. S. Schofield, E. Schwartz, D. Sellers, T. Shaffer, R. W. Short, D. Sigg, B. J. J. Slagmolen, C. Soike, S. Soni, V. Srivastava, L. Sun, D. B. Tanner, M. Thomas, P. Thomas, K. A. Thorne, M. R. Todd, C. I. Torrie, G. Traylor, A. S. Ubhi, G. Vajente, J. Vanosky, A. Vecchio, P. J. Veitch, A. M. Vibhute, E. R. G. von Reis, J. Warner, B. Weaver, R. Weiss, C. Whittle, B. Willke, C. C. Wipf, J. L. Wright, H. Yamamoto, L. Zhang, and M. E. Zucker. Advanced ligo detector performance in the fourth observing run. *Phys. Rev. D*, 111:062002, Mar 2025.
- [2] G. D. Cole, S. W. Ballmer, G. Billingsley, S. B. Cataño-Lopez, M. Fejer, P. Fritschel, A. M. Gretarsson, G. M. Harry, D. Kedar, T. Legero, C. Makarem, S. D. Penn, D. H. Reitze, J. Steinlechner, U. Sterr, S. Tanioka, G.-W. Truong, J. Ye, and J. Yu. Substrate-transferred gaas/algaas crystalline coatings for gravitational-wave detectors. *Applied Physics Letters*, 122(11):110502, 03 2023.
- [3] M. Evans, S. Ballmer, M. Fejer, P. Fritschel, G. Harry, and G. Ogin. Thermo-optic noise in coated mirrors for high-precision optical measurements. *Phys. Rev. D*, 78:102003, Nov 2008.
- [4] R. Kubo. The fluctuation-dissipation theorem. *Reports on Progress in Physics*, 29(1):255, jan 1966.
- [5] Yu. Levin. Internal thermal noise in the ligo test masses: A direct approach. *Phys. Rev. D*, 57:659–663, Jan 1998.
- [6] Stefan W. Ballmer. Photothermal transfer function of dielectric mirrors for precision measurements. *Phys. Rev. D*, 91:023010, 1 2015.
- [7] Tara Chalermongsak, Evan D. Hall, Garrett D. Cole, David Follman, Frank Seifert, Koji Arai, Eric K. Gustafson, Joshua R. Smith, Markus Aspelmeier, and Rana X. Adhikari. Coherent cancellation of photothermal noise in GaAs/Al<sub>0.92</sub>Ga<sub>0.08</sub>As Bragg mirrors. *Metrologia*, 53(2):860, April 2016.
- [8] Gregory M Harry, Matthew R Abernathy, Andres E

- Becerra-Toledo, Helena Armandula, Eric Black, Kate Dooley, Matt Eichenfield, Chinyere Nwabugwu, Akira Villar, D R M Crooks, Gianpietro Cagnoli, Jim Hough, Colin R How, Ian MacLaren, Peter Murray, Stuart Reid, Sheila Rowan, Peter H Sneddon, Martin M Fejer, Roger Route, Steven D Penn, Patrick Ganau, Jean-Marie Mackowski, Christophe Michel, Laurent Pinard, and Alban Remillieux. Titania-doped tantala/silica coatings for gravitational-wave detection. *Classical and Quantum Gravity*, 24(2):405, dec 2006.
- [9] Garrett D. Cole, Simon Gröblacher, Katharina Gugler, Sylvain Gigan, and Markus Aspelmeyer. Monocrystalline alxgal1-xas heterostructures for high-reflectivity high-q micromechanical resonators in the megahertz regime. *Applied Physics Letters*, 92(26):261108, 07 2008.
- [10] Garrett D. Cole, Wei Zhang, Michael J. Martin, Jun Ye, and Markus Aspelmeyer. Tenfold reduction of brownian noise in high-reflectivity optical coatings. *Nature Photonics*, 2013.
- [11] Garrett D. Cole, Wei Zhang, Bryce J. Bjork, David Follman, Paula Heu, Christoph Deutsch, Lindsay Sonderhouse, John Robinson, Chris Franz, Alexei Alexandrovski, Mark Notcutt, Oliver H. Heckl, Jun Ye, and Markus Aspelmeyer. High-performance near- and mid-infrared crystalline coatings. *Optica*, 3(6):647–656, Jun 2016.
- [12] Dahyeon Lee, Zoey Z. Hu, Ben Lewis, Alexander Aeppli, Kyungtae Kim, Zhibin Yao, Thomas Legero, Daniele Nicolodi, Fritz Riehle, Uwe Sterr, and Jun Ye. Frequency stability of  $2.5 \times 10^{-17}$  in a si cavity with AlGaAs crystalline mirrors, 2025.
- [13] S. Namba. Electro-optical effect of zincblende. . *Opt. Soc. Am.* 51, 76, 1961.
- [14] Satoshi Tanioka, Daniel Vander-Hyde, Garrett D. Cole, Steven D. Penn, and Stefan W. Ballmer. Study on electro-optic noise in crystalline coatings toward future gravitational wave detectors. *Physical Review D*, 107(2), January 2023.
- [15] Zhen Zhang and John T. Jr. Yates. Band bending in semiconductors: Chemical and physical consequences at surfaces and interfaces. *Chemical Reviews*, 112(10):5520–5551, 2012. PMID: 22783915.
- [16] Jialiang Yu, Sebastian Häfner, Thomas Legero, Sofia Herbers, Daniele Nicolodi, Chun Yu Ma, Fritz Riehle, Uwe Sterr, Dhruv Kedar, John M. Robinson, Eric Oelker, and Jun Ye. Excess noise and photoinduced effects in highly reflective crystalline mirror coatings. *Phys. Rev. X*, 13:041002, Oct 2023.
- [17] C Y Ma, J Yu, T Legero, S Herbers, D Nicolodi, M Kempkes, F Riehle, D Kedar, J M Robinson, J Ye, and U Sterr. Ultrastable lasers: investigations of crystalline mirrors and closed cycle cooling at 124 k. *Journal of Physics: Conference Series*, 2889(1):012055, nov 2024.
- [18] Tara Chalermsongsak, Evan D. Hall, Garrett D. Cole, David Follman, Frank Seifert, Koji Arai, Eric K. Gustafson, Joshua R. Smith, Markus Aspelmeyer, and Rana X. Adhikari. Coherent Cancellation of Photothermal Noise in GaAs/Al<sub>0.92</sub>Ga<sub>0.08</sub>As Bragg Mirrors. *Metrologia*, 53:860, 2016.
- [19] Eric D. Black. An introduction to pound–drever–hall laser frequency stabilization. *American Journal of Physics*, 69(1):79–87, 01 2001.
- [20] AlGaAs optical properties. <https://www.ioffe.ru/SVA/NSM/Semicond/AlGaAs/optic.html>.
- [21] V. Mitin, Lino Reggiani, and Luca Varani. Generation-recombination noise in semiconductors. *N/A*, 01 2002.
- [22] P. M. Mooney. Deep donor levels (dx centers) in iii-v semiconductors. *Journal of Applied Physics*, 67(3):R1–R26, 02 1990.
- [23] D. V. Lang and R. A. Logan. Large-lattice-relaxation model for persistent photoconductivity in compound semiconductors. *Phys. Rev. Lett.*, 39:635–639, Sep 1977.